



# A Test-Time Learning Approach to Reparameterize the Geophysical Inverse Problem with a Convolutional Neural Network

Anran Xu , Lindsey J. Heagy 

**Abstract**—Regularization is critical in solving the ill-posed geophysical inversion problems. Explicit regularization is often used, but there are opportunities to explore the implicit regularization effect inherently from a Neural Network structure. Researchers in Computer Vision (CV) have discovered that the Convolutional Neural Network (CNN) architecture inherently enforces a regularization that is advantageous for addressing diverse CV inverse problems, including de-noising and in-painting. In this study, we examine the applicability of this implicit regularization to geophysical inversions. The CNN maps an arbitrary vector to the model space (e.g., log-conductivity on the simulation mesh). The predicted subsurface model is then fed into a forward numerical simulation process to generate corresponding predicted measurements. Subsequently, the objective function value is computed by comparing these predicted measurements with the observed field measurements. The backpropagation algorithm is employed to update the trainable parameters of the CNN during the inversion. Note that the CNN in our proposed method does not require training before the inversion, rather, the CNN weights are estimated in the inversion algorithm, hence this is a test-time learning (TTL) approach. The results demonstrate that the implicit regularization provided by the CNN can be useful in DC resistivity inversions. We also provide a detailed discussion of the potential sources of this implicit regularization and some practical guides for applying the proposed method to other geophysical scenarios. The proposed approach for reparameterizing the inverse problem can be adapted to other Tikhonov-style geophysical inversions.

**Index Terms**—Convolutional neural network (CNN), deep image prior (DIP), deep learning (DL), direct-current resistivity inversion, and parameterized inversion (PI).

## I. INTRODUCTION

**G**EOPHYSICAL inversions are widely used in mining, environmental, and engineering applications [22], [25]. Because geophysical inversions are ill-posed, regularization is important for obtaining a geologically reasonable solution. A conventional approach employs the Tikhonov-regularized method where an explicit regularization term, comprised of smallness and smoothness, is included in the objective function [22]. The L2 norm is standard in the Tikhonov-regularized methods [3], but there is research on using different norms to promote sparse or compact structures [18]. Researchers also developed strategies for incorporating physical properties [28], [29] into the Tikhonov-regularized methods. The recent emergence of deep learning has garnered significant attention

from researchers, particularly regarding the integration of machine learning algorithms into the regularization [14], [24], [25], [30].

One main approach is to search for a solution in a latent space whose distribution contains prior information learned from the training samples [1]. For example, in the Ground-penetrating radar (GPR) inversion, Laloy *et al.* [6] and Lopez-Alvis *et al.* [9] trained Variational Autoencoders to map the distributions of the spatial patterns of the subsurface materials into simple distributions and integrated this learned prior into the objective function. In the seismic full-waveform inversion (FWI), Mosser *et al.* [10] trained a generative adversarial network with the knowledge of subsurface geology. These methods predict more realistic subsurface models. In the electromagnetic (EM) inversion problems, B. Liu *et al.* [7] proposed the method PhResNet [7], which reconstructs the subsurface model by a U-net. B. Liu *et al.* [7] stated that reconstructing the resistivity models with CNN is beneficial by showing the inversion results with a training dataset. Examining the potential benefits of reparameterizing the subsurface model without a training dataset is one motivating factor for our work. Both the utilization of generative models and PhResNet require a training dataset, which implies that we need prior knowledge of what we are looking for in the subsurface (e.g. the possible geological models or subsurface materials of the survey domain). Therefore, this approach utilizes a physically motivated prior.

Another approach employs so-called test-time learning (TTL) methods which do not require any training data when applied to each case. Rather than adjusting the weights of a neural network using training samples, the weights of a neural network are learned at the time the neural network is applied to the inversion process. TTL was first applied in the inverse problems in computer vision (CV). One example of the inverse problem in CV is in-painting (e.g. filling in corrupted portions of an image). This is achieved by learning the self-similarity between the corrupted image and the predicted image which is the output of the neural network. Researchers have found that some neural networks, such as Convolutional Neural Networks (CNNs) and Graph Convolutional Networks (GCNs), inherently enforce a regularization that is advantageous for addressing diverse CV inverse problems or mesh restoration problems [4], [17]. TTL methods have been applied to many biomedical imaging problems later [13], [26]. In geophysics, TTL has been employed in seismic FWI inversion by integrating the ML architecture into the inverse process in

Manuscript received November 28, 2023.

Anran Xu and Lindsey J. Heagy are with the Department of Earth, Ocean and Atmospheric Sciences, University of British Columbia, Vancouver, BC V6T 1Z4 Canada (email: anranxu@eoas.ubc.ca; lheagy@eoas.ubc.ca)

different ways [5], [11], [12], [15]. He *et al.* [5] and Wu *et al.* [11] reparameterized the velocity model into the CNN domain and attributed the regularization effect to the prior information learning by fitting the initial velocity models. In contrast, Zhu *et al.* [15] stated that this regularization effect comes from the CNN architectures as what Ulyanov *et al.* [17] proposed. Zhu *et al.* [15] examined this statement in the synthetic cases and found that this regularization effect is beneficial in cases where the noise is high. Utilizing trainable weights within the CNN to parameterize the subsurface model worked well to regularize the seismic inverse problems, but the prior they impose on the solution is not a physically motivated prior.

The physics that governs seismic FWI is the wave equation, and the strategies taken to solve the wave equation differ from those used in EM and potential field inversions, which are the so-called Tikhonov-style inversions. In this study, we would like to know the difference of the EM inversion results between the conventional Tikhonov-regularized methods and the methods with implicit regularization. In this work, we choose the direct current (DC) resistivity inversion, which is one type of EM inversion, but the proposed method can be applied to other Tikhonov-style geophysical inversions. Moreover, we explore the source of this implicit regularization effect and state that it is partly from the bi-linear upsampling operation, which smooths the final predicted model efficiently in some scenarios. Throughout, we will refer to this method as the Deep Image Prior Inversion (DIP-Inv), as it was inspired by the work of [17], which introduced the concept of the Deep Image Prior in computer vision.

We will begin with an overview of the methodology and describe the modifications we make to the pipeline of inversion. Then we will show the results using the DIP-Inv. The results illustrate that the CNN reparameterization provides useful regularization effects; therefore, DIP-Inv gives better inversion results than the conventional methods in some cases. After that, we explore different components of DIP-Inv and identify the bi-linear upsampling operation as one of the main sources of this implicit regularization effect.

The main contributions of our work include:

- 1) Compare inversion results obtained from conventional Tikhonov-regularized methods with sparse norms and obtained from the DIP-Inv approach on multiple synthetic examples to illustrate that the implicit regularization effect inherently from CNN is useful in the EM inversions.
- 2) Examine some key choices in the CNN architecture to illustrate that the bi-linear upsampling operation is one of the main sources of this implicit regularization effect and the Dropout technique is also useful.
- 3) Discuss some practical details for connecting the forward simulation, written in SimPEG [2], with PyTorch [21].

## II. METHODOLOGY

In this section, we will first compare the conventional method for solving the geophysical inverse problem and the proposed method (DIP-Inv). Then, we will illustrate the

structure of DIP-Inv. Finally, we will explain the objective function of the proposed method in detail. Note that we only conduct 2D DC resistivity inversions in this study, but this methodology can be adapted to 3D DC resistivity inversions or other Tikhonov-style geophysical inversions.

### A. Overview of the Conventional Inversion Method

In a DC resistivity survey, transmitters inject a steady-state electrical current into the ground and the receivers measure the resulting distribution of potentials (voltages) on the surface. The observation  $d^{obs} \in R^N$  consists of the potential differences between the two electrodes in each receiver and  $N$  is the number of transmitter-receiver pairs. The Poisson equation governs the physics of the DC resistivity experiment

$$\nabla \cdot \sigma \nabla \phi = \nabla \cdot \mathbf{j}_{source} \quad (1)$$

where  $\sigma$  is the electrical conductivity,  $\phi$  is the electric potential, and  $\mathbf{j}_{source}$  is the source current density. We solve this equation using a finite volume approach where we discretize the subsurface using a tensor mesh (c.f. [16]), which defines the 2D mesh space  $M$ . The mesh consists of a core region, with uniform cells, and padding regions on the lateral boundaries and the bottom of the mesh, with expanding cells to ensure boundary conditions are satisfied. We use SimPEG, an open-source package, to implement the forward modelling [2].

In a conventional Tikhonov-style inversion, we pose an optimization problem that seeks to minimize an objective function comprised of a data misfit term,  $\phi_d$ , and a regularization term,  $\phi_m$ . For the DC resistivity problem,  $m$  is chosen to be the log of the subsurface conductivity, and the inverse problem takes the form

$$\begin{aligned} \min_m \phi_d(m) + \beta \phi_m(m) = \\ \min_m \frac{1}{2} \|W_d(F(m) - d^{obs})\|^2 + \beta(\alpha_s \|W_s(m - m_{ref})\|^{p_s} + \\ \alpha_x \|W_x D_x m\|^{p_x} + \alpha_z \|W_z D_z m\|^{p_z}). \end{aligned} \quad (2)$$

The trade-off parameter  $\beta$  weights the relative importance of the data-misfit term and the regularization term. Often, a  $\beta$ -cooling strategy is adopted, and the value of the trade-off parameter  $\beta$  is gradually reduced as the inversion progresses [22]. The regularization term  $\phi_m$  generally includes a smallness term which penalizes the difference from a reference model  $m_{ref}$ , and a first-order smoothness term that penalizes spatial gradients in the model. The relative influence of each of these terms is weighted by the scalar parameters  $\alpha_{s,x,z}$ . The standard choice of norms in the regularization is  $p_{s,x,z} = 2$ , however, different norms where  $p_{s,x,z} \leq 2$  can be chosen, and we will use the implementation described in [18] for these inversions. Optionally, sensitivity weights can be included in the weight matrices  $W_{s,x,z}$ , and these have been shown to help improve the convergence of inversions where  $p_{s,x,z} \leq 2$ , [18].

The conventional approach for solving this inverse problem is by first initializing  $m \in M$  as the reference model  $m_{ref}$ , which is generally taken to be a uniform half-space, and iteratively updating  $m$  to reduce the value of the objective function. Various modifications can be made to the optimization problem in 2 when prior geologic information is

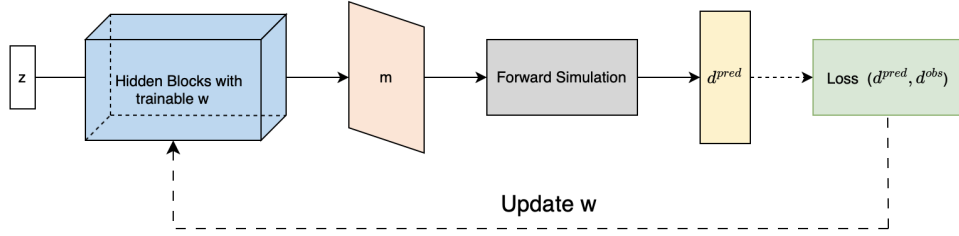


Fig. 1. Proposed parameterized inversion method. Compared with the conventional method, DIP-Inv reparameterizes the mesh space into the CNN-weights space.

available. When minimal information is available, the first-order smoothness terms generally play an important role in obtaining geologically reasonable results (e.g. [22]). In the work that follows, we choose inversion results with both smallness and first-order smoothness terms in the regularization as benchmarks for the conventional method.

### B. Overview of the Proposed Parameterized Inversion method-DIP-Inv

We are interested in exploring if implicit regularization can be advantageous in solving the inverse problem, so the main update that we make to the inverse problem posed in 2 is that we parameterize the model in terms of a CNN-based function.

In our proposed method, a CNN-based function  $L$ , whose weights are denoted as  $w$ , maps an arbitrary vector  $z \in R^k$  to a model  $m$  in the mesh space  $M \in R^{W \times H}$  (See Fig. 1).

$$L_w(z) = m. \quad (3)$$

Note that the padding cells are included in  $m$ . The predicted subsurface model  $m$  is then fed into the forward numerical simulation to generate the corresponding predicted measurements  $d^{pred}$ . The modified optimization problem that we aim to solve is

$$\begin{aligned} & \min_w (1 - \beta)\phi_d + \beta\phi_m = \\ & \min_w \frac{(1 - \beta)}{2} \|W_d(F(L_w(z)) - d^{obs})\|^2 + \\ & \beta \|L_w(z) - m_{ref}\|^1. \end{aligned} \quad (4)$$

Compared with the supervised end-to-end machine learning methods in the EM inversion [27], DIP-Inv imposes physical constraints in the forward simulation. Compared with the conventional Tikhonov-regularized methods, the objective function in the proposed method doesn't have the smoothness term since the smoothness constraint is implicitly included in the upsampling operator in  $L$  (section IV-A). Also, we remove the sensitivity weighting from the regularization without deteriorating the inversion results. The backpropagation algorithm, which is implemented by PyTorch, is employed to update the trainable parameters  $w$  in function  $L$ . Since the weights  $w$  are randomly initialized, the start model  $m = L_w(z)$  won't be  $m_{ref}$  without pre-training. In the first stage of DIP-Inv, we update the weights  $w$  with the objective function  $\|m - m_{ref}\|^1$  to make the start model for the second stage similar to the start model of the conventional method. In the second stage,

we load the pre-trained weights first and then update the weights with the objective function 4. Note that the implicit regularization effect does not come from the pre-trained since the reference model is a uniform half-space. Stage one is mainly to save time: The pre-trained weights in the first stage can be stored and reused for future experiments with the same reference model.

### C. Architecture of DIP-Inv

The structure of the function  $L$  is illustrated in Fig 2. The input  $z$  is a fixed 1D vector sampled from the Gaussian distribution with mean 0 and standard deviation 10 and is not trainable. The first hidden block is a multi-layer perceptron (MLP) whose output is  $y_1 \in R^h$ , and the value of  $h$  should be adjusted to adapt different mesh designs (i.e. dimension of  $M$ ). Sequentially,  $y_1$  is reshaped and then fed into 3 hidden blocks where each block has an upsampling layer, a 2D convolutional layer, and a Leaky ReLU activation layer. The last hidden layer only has a 2D convolutional layer followed by a sigmoid activation function. The output of the CNN is cropped to have the same dimension as  $M$ . Sigmoid activation will squeeze the output into  $(0, 1)$ . Since we perform the forward modelling on a log-conductivity scale, all elements in the output of the last hidden layer are multiplied by -8 before being fed into the forward simulation. Namely, we assume that the subsurface space has conductivity with range  $(\exp(-8), \exp(0))$  S/m  $\approx (3.35e-4, 1)$  S/m, which covers a large range of natural subsurface materials. This multiplier can be changed to different values to adapt to different conductivity ranges. The dropout layer can also be included in the second stage and we will examine the impact of the regularization effect from the Dropout layer in section IV-C. Although some advanced machine learning models for 2D data use components such as inception blocks, skip connections and residual blocks, they are often based on a CNN architecture. Our DIP-Inv method is also CNN-based and provides a good test for exploring the utility of the implicit regularization effect. As a result, testing this basic model structure is a good first choice in exploring the utility of the implicit regularization effect.

### D. Necessary Explicit Regularization in DIP-Inv

One of the main purposes of this study is to test the implicit regularization effect introduced by the CNN structures. Although one might be inclined to try to eliminate all explicit regularization, this is a very ill-posed problem,

and we find that including the smallness term is important for this problem. Thus, we choose to analyze the impacts of the implicit regularization effects of a CNN as compared to the role of the explicit smoothness terms in the conventional approach.

The other modification that we make is in how we treat the trade-off parameter  $\beta$ . The trade-off parameter  $\beta$  in the proposed method is an exponential decay function.

$$\beta = e^{-\frac{t}{\tau}}, \quad (5)$$

where  $t$  is the index for the epochs and  $\tau$  is a constant decay rate. Namely,  $\beta = e^{-\frac{t}{\tau}}$  in the  $i$ -th epoch. Although the conventional method uses a different cooling schedule and doesn't employ  $(1 - \beta)$  in front of the  $\phi_d$ , we have found that this choice of cooling schedule performs well with the proposed method.

### E. A practical implementation techniques

We choose Adam [19] as the optimizer for the DIP-Inv. Adam updates  $w$  based on the gradient of the objective function, so we need to make sure that the gradient is correctly calculated. Let's denote the objective function in 4 as  $\mathcal{L} = (1 - \beta)\phi_d + \beta\phi_m$ . Note that we use the convention of column vector in this subsection.

$$\begin{aligned} \frac{\partial \mathcal{L}}{\partial w_i} &= (1 - \beta) \frac{\partial \phi_d}{\partial w_i} + \beta \frac{\partial \phi_m}{\partial w_i} \\ &= (1 - \beta) (\nabla_m \phi_d)^T \frac{\partial m}{\partial w_i} + \beta \frac{\partial \phi_m}{\partial w_i} \\ &= (1 - \beta) J_v^T \frac{\partial m}{\partial w_i} + \beta \frac{\partial \phi_m}{\partial w_i}. \end{aligned} \quad (6)$$

DIP-Inv uses SimPEG for the forward simulation and PyTorch for building the CNN architecture. We need to connect SimPEG (computing  $J_v = \nabla_m \phi_d$ ) with PyTorch (automatic differentiate  $w$ ). Here we play a trick: We define  $\mathcal{L}' = (1 - \beta^t)(J_v^T m^t) + \beta^t \|m^t - m_{ref}\|^1$  and  $J_v^T$  is considered as a fixed vector when calling  $\mathcal{L}'.backward()$  and  $optimizer.step()$  to update the weights  $w$  in CNN. Although  $L$  and  $L'$  are not identical, their gradients with respect to the weights  $w$  are the same. Here, we elaborate on how we implement it:

### Algorithm 1 Integrating SimPEG to the Optimization Process.

---

**Input:**  $\tau, W, z, d^{obs}, m_{ref}, w^t$ , and hyperparameters for  $L$   
**for**  $t = 1$  **to** ... **do**  
  Compute  $\beta^t = e^{-\frac{t}{\tau}}$   
  Compute  $m^t = L_{w^t}(z)$   
  Compute  $J_v = \nabla_m \phi_d|_{m=m^t}$   
  using *simulation.Jtvec*( $m, W_d^T W_d(d^{pred} - d^{obs})$ )  
  from SimPEG  
  Compute  $\mathcal{L}' = (1 - \beta^t)(J_v^T m^t) + \beta^t \|m^t - m_{ref}\|^1$   
  Update  $w_t$  using  $\mathcal{L}'.backward()$  and *optimizer.step()*

---

## III. TRIALS ON THE SYNTHETIC CASES

In this section, we will consider two synthetic models and perform inversions using both the conventional Tikhonov-regularized methods and the proposed DIP-Inv method. The main target for Case 1 is a conductive dike under a less conductive near-surface layer. The main targets for Case 2 are two structures in close proximity. To generate the synthetic observations, we use the same survey configuration and mesh design with 5% Gaussian noise. By comparing the inversion result from the conventional and proposed methods, we will show that the proposed method provides a useful smoothness effect (Case 1) and can better distinguish the compact anomalies (Case 2). Note that L2 norms always promote more blurred structures compared to sparse norms; therefore, we choose the results from the conventional method with sparse norms as benchmarks.

### A. Survey Configuration and Mesh Design

We chose a dipole-dipole survey geometry with a station separation of 25 meters and a maximum of 24 receivers per transmitter. The survey line is 700 meters long, so the total number of potential difference measurements is  $348 (= 3 \times 24 + (23 + 1) \times 23/2)$ .

For the simulation, we use a mesh that has core cells of  $5m \times 5m$ , with 200 core-mesh cells in the x-direction and 25 cells in the z-direction. We add 7 padding cells that extend by a factor of 1.5 to the sides and bottom of the mesh. In total, the mesh has  $W \times H = 6944$  cells. The total number of trainable weights in  $L$  is 23055 based on the DIP-Inv architecture (see the Appendix for details), so we over-parameterize the problem. We also add a dropout layer to impose a stronger net regularization effect on this over-parameterized problem (see section IV-C). The subsurface conductivity models for Case 1 and Case 2 are shown in Fig. 3 and Fig. 4.

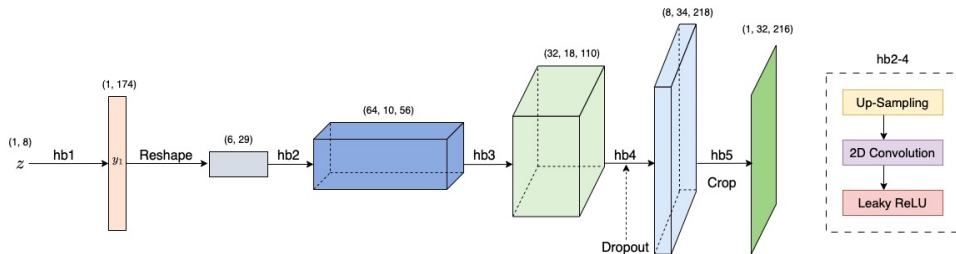


Fig. 2. Architecture of DIP-Inv. The structure of hidden blocks 2-4 is shown on the right (hb denotes hidden block). More details are shown in the Appendix.

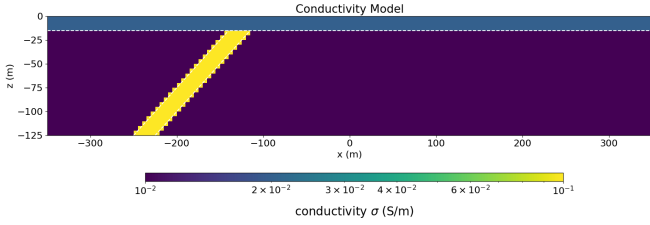


Fig. 3. True Model for Case 1. The top layer has a conductivity of 0.02 S/m. The dike, with a dip angle of 45 degrees, has a conductivity of 0.1 S/m. The background has a conductivity of 0.01 S/m.

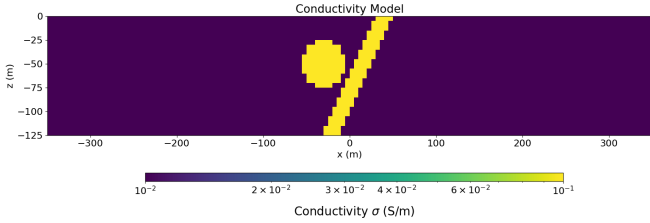


Fig. 4. True Model for Case 2. The cylinder and the dike have a conductivity of 0.1 S/m. The background has a conductivity of 0.01 S/m.

### B. Choice of optimization method

In the proposed method, we choose Adam, a first-order optimizer, with a learning rate of 0.0001 to update  $w$  in  $L$ . Note that the conventional method uses Inexact Gaussian Newton [23], a second-order optimization method, to update  $m$ , since second-order optimization methods are known to speed up convergence for a variety of inverse problems [3]. However, researchers find practical challenges in employing second-order optimization methods to train a Neural Network (NN) partly because estimating the Hessian would be time-consuming in the case where the number of trainable parameters in an NN is large [8].

### C. Case 1

We first find the best conventional inversion results with respect to the true model by conducting multiple conventional inversions using different values of  $p_s$ ,  $\alpha_i$ , and  $p_i$  ( $i = x$  or  $z$ ) with or without sensitivity weighting.

We find that the best conventional inversion results with respect to the true models are from  $p_s = 0$ ,  $p_x = p_z = 1$ ,  $\alpha_s = 0.005$ , and  $\alpha_x = \alpha_z = 0.5$ . See Fig. 5. We perform the proposed method with a decay rate of  $\tau = 1000$ , and a dropout rate of 0.1 after the fourth hidden block.

All models fit the data to a comparable level, and the  $\chi$ -factor (the ratio of the final misfit with the target misfit, c.f. [22]) of each model is shown in the bottom right-hand-side of each inversion result. Though each shows a conductive, dipping structure, the details differ. In Figure 5b, we can see that by not including sensitivity weighting, we recover a more diffuse structure. We also see near-surface artifacts where we have high sensitivity to the electrode locations. Using sensitivity weighting, as shown in Figure 5c, reduces the near-surface artifacts and improves the recovery of the near-surface conductive layer. The dike structure is better defined, but the dip is more vertical than the true model. The DIP-Inv

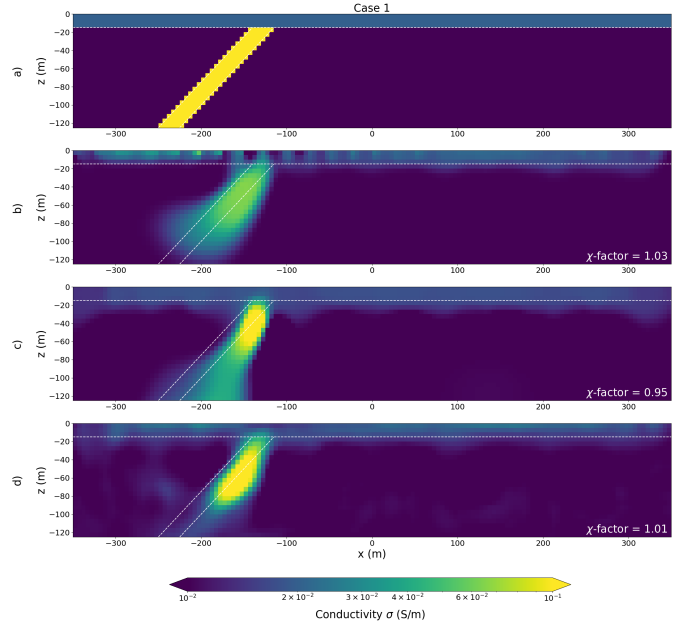


Fig. 5. (a) is the true conductivity model for Case 1. (b) and (c) are the conventional inversion results without/with sensitivity weighting, respectively. (d) is the DIP-Inv result.

result (Figure 5d) does not require any sensitivity weighting and shows an improved recovery of the dip of the dike. We also recover the near-surface layer as a smooth structure.

To further test the recovery of the dip angle, we perform two other sets of inversions with two different true models that have different dip angles (See Case 1.2 and Case 1.3 in Fig. 6). The proposed method recovers the top layer well and surpasses the conventional method in terms of recovery of the dip angle.

### D. Case 2

We perform a set of conventional inversions and find that  $p_s = 0$ ,  $p_x = p_z = 2$ ,  $\alpha_s = 0.005$ , and  $\alpha_x = \alpha_z = 0.5$  give the best conventional results with respect to the true model in Case 2. We then perform the proposed method with decay rate  $\tau = 800$ , and the dropout rate 0.05 after the fourth hidden block. Again, all models fit the data to a comparable level. In Fig. 7b, c, the predicted models recover the cylindrical structure and a thin dike-like structure near the surface, but the structure of the dike doesn't extend to depth. As a contrast, the DIP-Inv result (Fig. 7d) recovers the dike, and it is clear that it extends at depth, we also see the cylindrical target being recovered at the correct location, though its amplitude is reduced as compared to the true model.

To further verify the argument that the DIP-Inv method can distinguish the two compact anomalies in close proximity. We conduct another trial on a model with two compact, cylindrical targets (see Fig. 8a). Using the conventional approach without sensitivity weighting (Fig. 8b), we recover a blurred model that connects the two structures. Using sensitivity weighting is an improvement and we can see that there are two distinct anomalous bodies. They are somewhat smeared vertically (Fig. 8c). The DIP-Inv result arguably provides the best recovery of

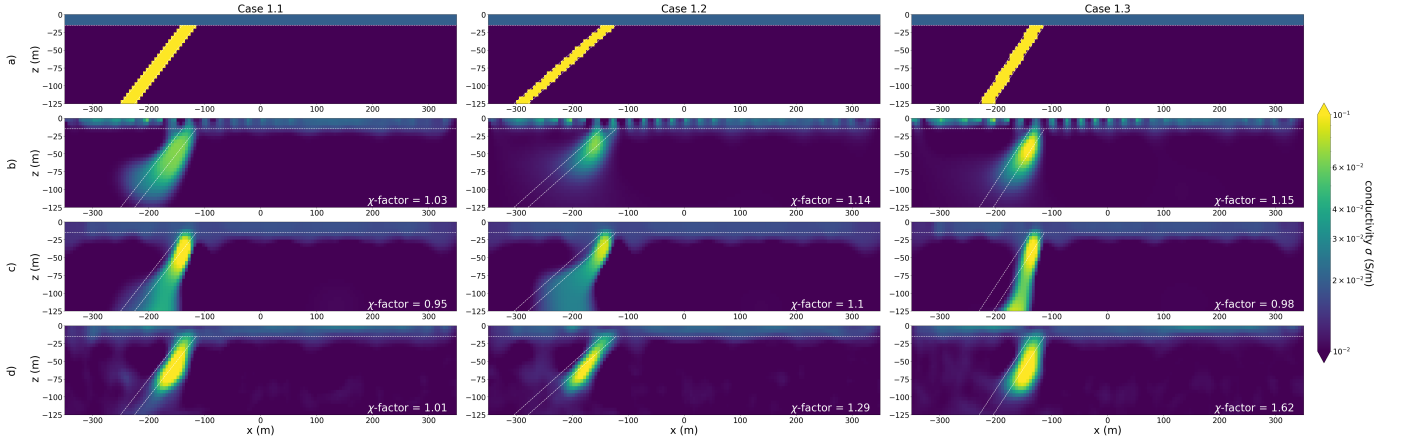


Fig. 6. (a) is the true model; the dip of the dike is varied. (b) and (c) are from the conventional sparse-norms inversions without/with sensitivity weights respectively. (d) is the DIP-Inv result.

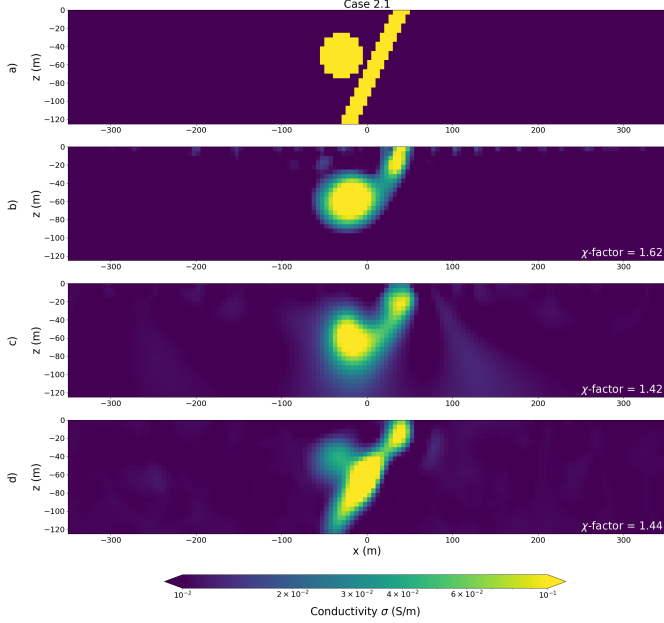


Fig. 7. (a) is the true model for Case 2.1. (b) and (c) are from the conventional sparse-norms inversions without/with sensitivity weights respectively. (d) is the DIP-Inv result.

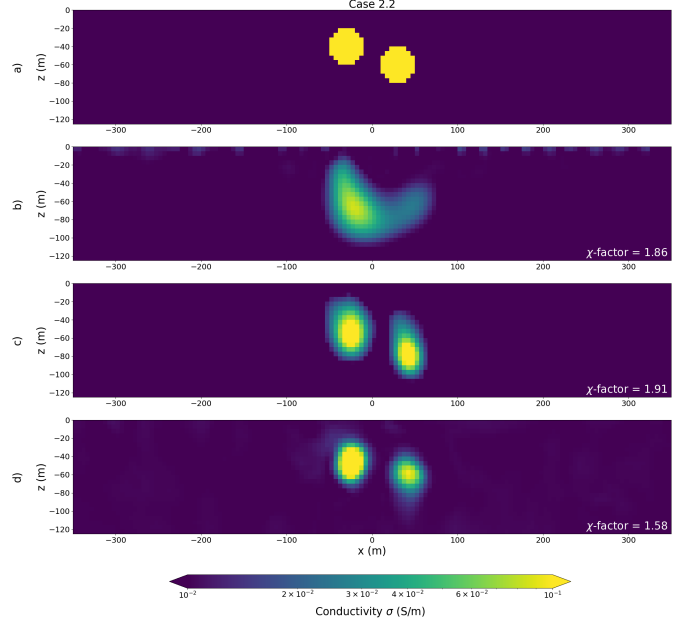


Fig. 8. (a) is the true model for Case 2.2. (b) and (c) are from the conventional sparse-norms inversions without/with sensitivity weights respectively. (d) is the DIP-Inv result.

the two compact targets (Fig. 8d). Together, Cases 2.1 and 2.2 show that the DIP-Inv approach is beneficial for recovering compact targets that are in close proximity to one another.

#### IV. IMPLICIT REGULARIZATION IN DIP-INV

In this section, we will explore the implicit regularization effect observed in the recovery models from the proposed method. We hypothesize that the smoothing effect generated by the bi-linear upsampling operator is a key component of the DIP-Inv approach. We test this hypothesis by replacing bi-linear upsampling with other upsampling operators. Finally, we present the effect of changing the number of hidden blocks and adding dropout layers.

#### A. Bi-linear Upsampling Operator

In this subsection, we test the hypothesis that the observed implicit regularization effect is mainly from the bi-linear upsampling operator. The bi-linear upsampling is a common choice for up-scaling the dimension of certain hidden layers. If we consider that the  $i$ th hidden layer is a bi-linear upsampling layer with upsampling scale  $k$  and input dimension  $(a, b, c, d)$ , then the output dimension for the  $i$ th hidden layer is  $(a, b, kc, kd)$ . The bi-linear interpolation is employed in this up-scaling process.

The output value of the bi-linear interpolation in each pixel is a distance-based, weighted sum of the surrounding pixels; therefore, bi-linear interpolation generates a pixel-level smoothed output. To verify our hypothesis, we replace the bi-linear upsampling with the nearest neighbour upsampling or

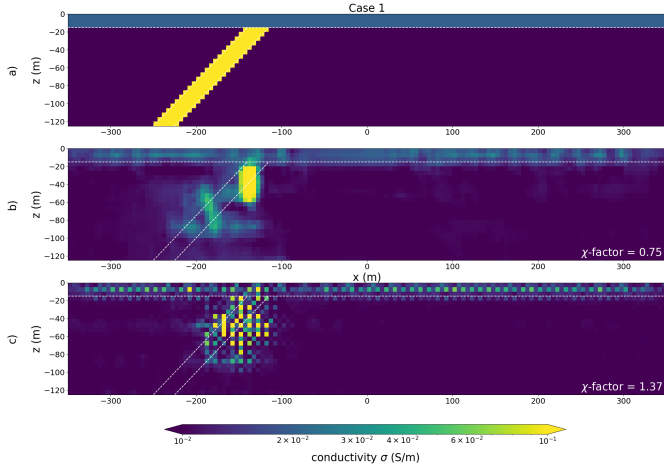


Fig. 9. (a) is the true model for Case 1.1. (b) and (c) are from inversion using nearest neighbour upsampling and transposed convolution operator respectively.

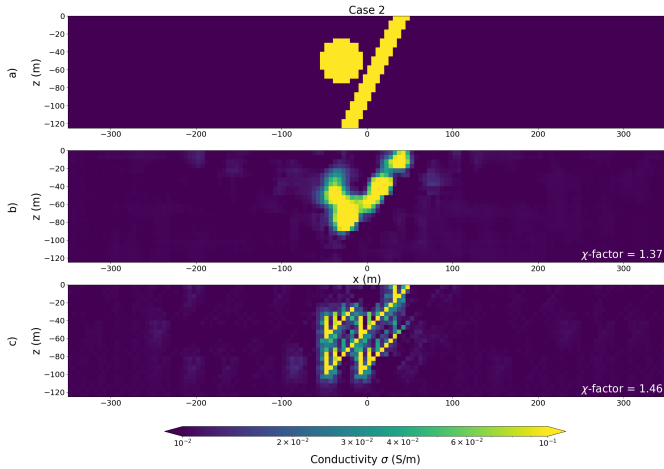


Fig. 10. (a) is the true model for Case 2.1. (b) and (c) are from inversion using nearest neighbour upsampling and transposed convolution operator respectively.

a transposed convolution. Our experiments demonstrated that these alternatives yielded inferior results (see Fig. 9 and 10), which supports that the bi-linear interpolation is critical in the success of DIP-Inv.

### B. Choice of architecture

To further test our hypothesis that the implicit regularization effect is partly from the bi-linear upsampling operator, we show the results from changing the number of bi-linear upsampling layers by two in the DIP-Inv. Since we argue that the implicit effect partially comes from the bi-linear upsampling layers, the regularization effect should be amplified as we increase the number of hidden blocks (one hidden block has one bi-linear upsampling layer), and vice versa. Similar to the need to choose a good trade-off between the data misfit term and the regularization term in the conventional method, we need to choose how much regularization effect we want to impose for our DIP-Inv method. Too much or too little regularization is both problematic.

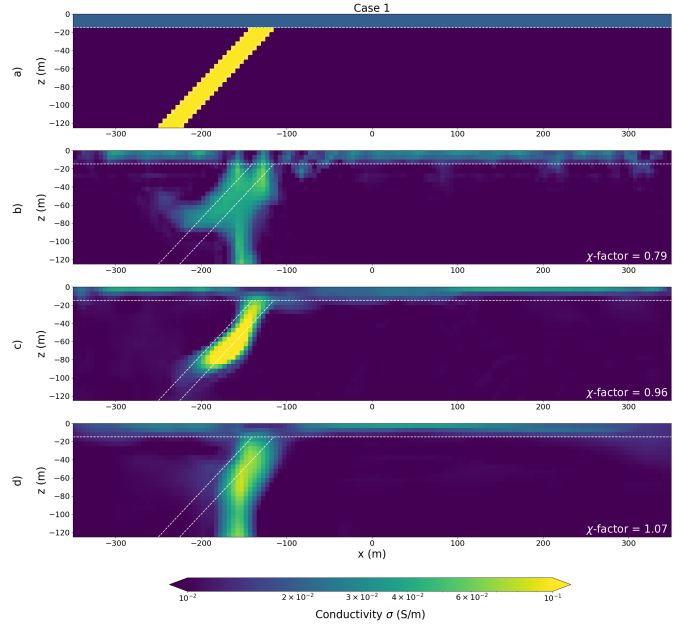


Fig. 11. (a) is the true model. (b), (c), and (d) are results for employing 1, 3, and 5 hidden blocks respectively. All results are from the CNN architectures without a dropout layer.

The DIP-Inv inversion results for Case 1 using 1, 3 and 5 hidden blocks are shown in Figure 11. We choose to not use a dropout layer in this subsection to avoid ambiguity on the source of the regularization effect. Using only one hidden block (Fig. 11b), we recover a model with lots of structure and artifacts, illustrating that one hidden block is insufficient for providing the regularization effect. On the other hand, when we use five hidden blocks, we recover a more blurred structure (Fig. 11d) because the additional hidden blocks provide more regularization. For this model, we find that using three hidden blocks (Fig. 11c) provides an appropriate level of regularization for this model. Note that the optimal number of layers will depend upon the subsurface model. We repeat this experiment for the model from Case 2 to support our conclusion and show these results in Fig. 12. Again, we see that increasing the number of hidden blocks increases the regularization effect, and for this model, using three layers provides an appropriate level of regularization.

### C. Enhanced Smoothing Effects from the Dropout Layer

Dropout is used to prevent the over-fitting issue in training large neural networks [20]. It surpasses conventional regularization methods such as Tikhonov regularization and max-norm regularization in supervised tasks in computer vision, speech recognition, etc [20]. When using dropout, we randomly zero out certain neurons during each training epoch; since different neurons are chosen to be zero-outed in each epoch, this is a stochastic regularization method. Intuitively, this stochastic zero-out scheme prevents the final output from relying too much on any particular neuron. Therefore, it improves the generalization of the neural network. If you view dropout as a model sampling method, in each epoch, it will sample a new CNN model with different zero-outed

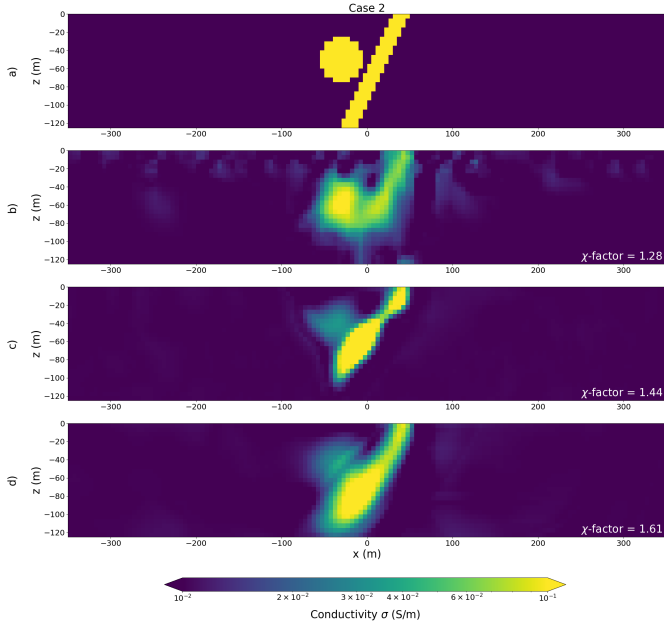


Fig. 12. (a) is the true model. (b), (c), and (d) are results for employing 1, 3, and 5 hidden blocks respectively. All results are from the CNN architectures without a Dropout layer.

neurons than the model in the last epoch, so the output of the last epoch would be approximately a weighted average of different models [20]. See Fig. 13 and 14 for an ablation study on having/not having a dropout layer in Case 1 and 2, respectively. We choose a dropout rate of 0.1 and only add 1 dropout layer after the fourth hidden block of the DIP-Inv.

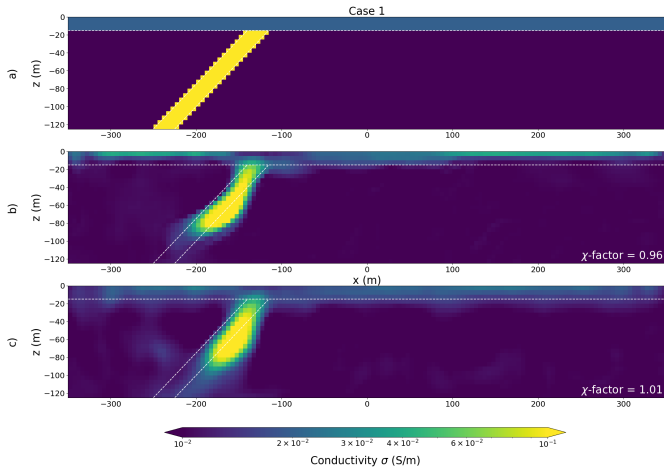


Fig. 13. (a) is the true model for Case 1. (b) is the inversion result from the proposed methods without a dropout layer, and (c) is the inversion result from the proposed methods with a dropout layer.

The dropout layer is useful for improving the recovery of the top layer of the subsurface for Case 1 as shown in Fig. 13 and recovery of the cylindrical target for Case 2 as shown in Fig. 14. A practical guide for applying the proposed method would be to perform the proposed method without the dropout layer in the first attempt, and then perform the proposed method with the dropout if the first result is not satisfying.

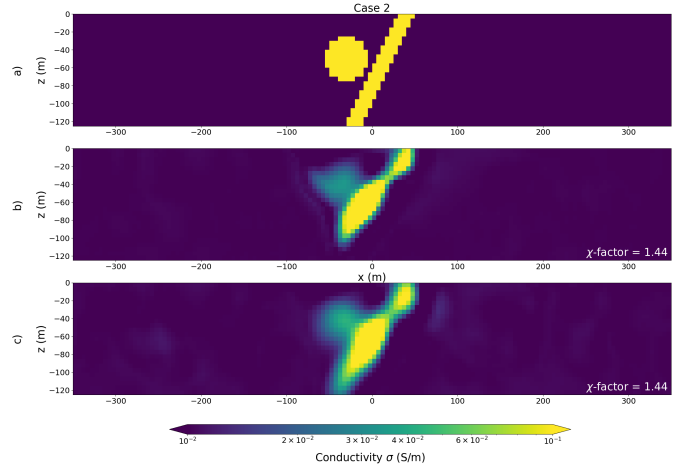


Fig. 14. (a) is the true model for Case 2.1. (b) is the inversion result from the proposed methods without a dropout layer, and (c) is the inversion result from the proposed methods with a dropout layer.

## V. FUTURE WORK

The idea of reparameterizing the mesh space can be adapted to other Tikhonov-style geophysical inversion problems (e.g. potential fields and electromagnetics, where SimPEG has other simulations that could be swapped in.). This method can also be combined with additional explicit regularization terms such as using a non-uniform reference model based on the petrophysical knowledge for the survey domain. Currently, the DIP-Inv method requires more than 1000 iterations, so it is much slower than a conventional inversion. Exploring more efficient optimizers is a direction of future research. Moreover, to illustrate the impacts of the implicit regularization on models with known structures, we only show the simple synthetic cases. Future work could also include examining the results of field data. Similarly, we chose to work with a simple CNN architecture, but exploring more complex architectures would be an avenue for further research.

## VI. CONCLUSION

Motivated by the work of utilizing the implicit regularization in the inverse problems in other fields, we explore the utility of the implicit regularization inherently included in the CNN structure for the Tikhonov-style geophysical inversion. In this study, we focus on the DC resistivity with synthetic examples and compare the DIP-Inv results with the conventional Tikhonov-regularized inversion results using the sparse norms. Compared to the conventional method, the DIP-Inv method improves the recovery of the dip of a target and the recovery of the compact targets in close proximity. We also show that the bi-linear upsampling operator is a key component in DIP-Inv and adding dropout can also have advantages in some cases. Those results illustrate that the implicit regularization from the CNN structure can be beneficial for the Tikhonov-style geophysical inversion. As a test-time learning method, DIP-Inv can be adapted to other geophysical inversion problems or combined with explicit regularization terms.



## DATA AVAILABILITY

The code used is available at  
<https://doi.org/10.5281/zenodo.10289234>.

## ACKNOWLEDGMENTS

We thank Jorge Lopez-Alvis for his comments and suggestions on paper writing. We would also like to thank Doug Oldenburg, Devin Cowan, Joseph Capriotti, John M. Weis, Johnathan C. Kuttai, Jingrong Lin and Santiago Soler for their invaluable guidance and advice on the use of SimPEG.

## APPENDIX

## DETAILS OF THE DIP-INV

As we mentioned in the paper, the dimension of  $y_1$  and other blocks should change to adapt the mesh design. For the two synthetic cases, where they share the same mesh design, we list the details of the hidden blocks in the Table below.

TABLE I

DETAILS OF THE ARCHITECTURES IMPLEMENTED IN THE TWO SYNTHETIC CASES

hb1	FC (8, 174) LeakyReLU (negative slope 0.2) reshape (1,1,6,29)
hb2	Bi-linear upsampling ( $k = 2$ ) Convolutional ((1,64), kernel ( $3 \times 3$ ), stride (1), padding (0)) LeakyReLU (negative slope 0.2)
hb3	Bi-linear upsampling ( $k = 2$ ) Convolutional ((64, 32), kernel ( $3 \times 3$ ), stride (1), padding (0)) LeakyReLU (negative slope 0.2)
hb4	Bi-linear upsampling ( $k = 2$ ) Convolutional ((32, 8), kernel ( $3 \times 3$ ), stride (1), padding (0)) LeakyReLU (negative slope 0.2)
hb5	Convolutional ((8, 1), kernel ( $3 \times 3$ ), stride (1), padding (0)) Sigmoid
output	cropped, $\times - 8$

## REFERENCES

- [1] A. Bora, A. Jalal, E. Price, and A. G. Dimakis, "Compressed Sensing using Generative Models." arXiv, Mar. 09, 2017. Accessed: Nov. 24, 2023. [Online]. Available: <http://arxiv.org/abs/1703.03208>
- [2] R. Cockett, L. J. Heagy, and D. W. Oldenburg, "Pixels and their neighbors: Finite volume," *The Leading Edge*, vol. 35, no. 8, pp. 703–706, Aug. 2016, doi: 10.1190/tle35080703.1.
- [3] E. Haber, U. M. Ascher, and D. Oldenburg, "On optimization techniques for solving nonlinear inverse problems," *Inverse Problems*, vol. 16, no. 5, pp. 1263–1280, Oct. 2000, doi: 10.1088/0266-5611/16/5/309.
- [4] S. Hattori, T. Yatagawa, Y. Ohtake, and H. Suzuki, "Deep Mesh Prior: Unsupervised Mesh Restoration using Graph Convolutional Networks." arXiv, Nov. 01, 2021. Accessed: Oct. 04, 2023. [Online]. Available: <http://arxiv.org/abs/2107.02909>
- [5] Q. He and Y. Wang, "Reparameterized full-waveform inversion using deep neural networks," *GEOPHYSICS*, vol. 86, no. 1, pp. V1–V13, Jan. 2021, doi: 10.1190/geo2019-0382.1.
- [6] E. Laloy, R. Héroult, J. Lee, D. Jacques, and N. Linde, "Inversion using a new low-dimensional representation of complex binary geological media based on a deep neural network," *Advances in Water Resources*, vol. 110, pp. 387–405, Dec. 2017, doi: 10.1016/j.advwatres.2017.09.029.
- [7] B. Liu *et al.*, "Physics-Driven Deep Learning Inversion for Direct Current Resistivity Survey Data," *IEEE Trans. Geosci. Remote Sensing*, vol. 61, pp. 1–11, 2023, doi: 10.1109/TGRS.2023.3263842.
- [8] H. Liu, Z. Li, D. Hall, P. Liang, and T. Ma, "Sophia: A Scalable Stochastic Second-order Optimizer for Language Model Pre-training." arXiv, May 23, 2023. Accessed: Jun. 21, 2023. [Online]. Available: <http://arxiv.org/abs/2305.14342>
- [9] J. Lopez-Alvis, F. Nguyen, M. C. Looms, and T. Hermans, "Geophysical Inversion Using a Variational Autoencoder to Model an Assembled Spatial Prior Uncertainty," *JGR Solid Earth*, vol. 127, no. 3, p. e2021JB022581, Mar. 2022, doi: 10.1029/2021JB022581.
- [10] L. Mosser, O. Dubrule, and M. J. Blunt, "Stochastic seismic waveform inversion using generative adversarial networks as a geological prior." arXiv, Jun. 10, 2018. Accessed: Nov. 18, 2023. [Online]. Available: <http://arxiv.org/abs/1806.03720>
- [11] Y. Wu and G. A. McMechan, "Parametric convolutional neural network-domain full-waveform inversion," *GEOPHYSICS*, vol. 84, no. 6, pp. R881–R896, Nov. 2019, doi: 10.1190/geo2018-0224.1.
- [12] F. Yang and J. Ma, "FWIGAN: Full-Waveform Inversion via a Physics-Informed Generative Adversarial Network," *JGR Solid Earth*, vol. 128, no. 4, p. e2022JB025493, Apr. 2023, doi: 10.1029/2022JB025493.
- [13] J. Yoo, K. H. Jin, H. Gupta, J. Yerly, M. Stuber, and M. Unser, "Time-Dependent Deep Image Prior for Dynamic MRI," *IEEE Trans. Med. Imaging*, vol. 40, no. 12, pp. 3337–3348, Dec. 2021, doi: 10.1109/TMI.2021.3084288.
- [14] S. Yu and J. Ma, "Deep Learning for Geophysics: Current and Future Trends," *Reviews of Geophysics*, vol. 59, no. 3, p. e2021RG000742, Sep. 2021, doi: 10.1029/2021RG000742.
- [15] W. Zhu, K. Xu, E. Darve, B. Biondi, and G. C. Beroza, "Integrating Deep Neural Networks with Full-waveform Inversion: Reparametrization, Regularization, and Uncertainty Quantification." arXiv, Sep. 30, 2021. Accessed: May 02, 2023. [Online]. Available: <http://arxiv.org/abs/2012.11149>
- [16] E. Haber, S. for Industrial, and A. Mathematics, *Computational Methods in Geophysical Electromagnetics*. Society for Industrial and Applied Mathematics.
- [17] D. Ulyanov, A. Vedaldi, and V. Lempitsky, "Deep Image Prior," *Int J Comput Vis*, vol. 128, no. 7, pp. 1867–1888, Jul. 2020, doi: 10.1007/s11263-020-01303-4.
- [18] D. Fournier and D. W. Oldenburg, "Inversion using spatially variable mixed Lp norms," *Geophysical Journal International*, vol. 218, no. 1, pp. 268–282, Mar. 2019, doi: 10.1093/gji/ggz156.
- [19] D. P. Kingma and J. Ba, "Adam: A Method for Stochastic Optimization." arXiv, Jan. 29, 2017. Accessed: Nov. 24, 2023. [Online]. Available: <http://arxiv.org/abs/1412.6980>
- [20] N. Srivastava, G. Hinton, A. Krizhevsky, I. Sutskever, and R. Salakhutdinov, "Dropout: A Simple Way to Prevent Neural Networks from Overfitting".
- [21] A. Paszke *et al.*, "PyTorch: An Imperative Style, High-Performance Deep Learning Library." arXiv, Dec. 03, 2019. Accessed: Nov. 25, 2023. [Online]. Available: <http://arxiv.org/abs/1912.01703>
- [22] D. K. Butler, Ed., *Near-Surface Geophysics*. Society of Exploration Geophysicists, 2005. doi: 10.1190/1.9781560801719.
- [23] J. Nocedal and S. J. Wright, *Numerical optimization*. in Springer series in operations research. New York: Springer, 1999.
- [24] Y. Hu, X. Wei, X. Wu, J. Sun, Y. Huang, and J. Chen, "3D cooperative inversion of airborne magnetic and gravity gradient data using deep learning techniques," *GEOPHYSICS*, pp. 1–57, Oct. 2023, doi: 10.1190/geo2023-0225.1.
- [25] T. Alyousuf, Y. Li, and R. Krahenbuhl, "Machine learning inversion of time-lapse three-axis borehole gravity data for CO2 monitoring," in Second International Meeting for Applied Geoscience & Energy, Houston, Texas: Society of Exploration Geophysicists and American Association of Petroleum Geologists, Aug. 2022, pp. 3099–3103. doi: 10.1190/image2022-3745388.1.
- [26] R. Liu, Y. Sun, J. Zhu, L. Tian, and U. Kamilov, "Recovery of Continuous 3D Refractive Index Maps from Discrete Intensity-Only Measurements using Neural Fields." arXiv, Aug. 14, 2022. Accessed: Nov. 29, 2023. [Online]. Available: <http://arxiv.org/abs/2112.00002>

- [27] M. R. Asif, N. Foged, T. Bording, J. J. Larsen, and A. V. Christiansen, "DL-RMD: a geophysically constrained electromagnetic resistivity model database (RMD) for deep learning (DL) applications," *Earth Syst. Sci. Data*, vol. 15, no. 3, pp. 1389–1401, Mar. 2023, doi: 10.5194/essd-15-1389-2023.
- [28] J. Sun and Y. Li, "Multidomain petrophysically constrained inversion and geology differentiation using guided fuzzy c -means clustering," *GEOPHYSICS*, vol. 80, no. 4, pp. ID1–ID18, Jul. 2015, doi: 10.1190/geo2014-0049.1.
- [29] T. Astic and D. W. Oldenburg, "A framework for petrophysically and geologically guided geophysical inversion using a dynamic Gaussian mixture model prior," *Geophysical Journal International*, vol. 219, no. 3, pp. 1989–2012, Dec. 2019, doi: 10.1093/gji/ggz389.
- [30] M. Eliasof, E. Haber, and E. Treister, "DRIP: deep regularizers for inverse problems," *Inverse Problems*, vol. 40, no. 1, p. 015006, Jan. 2024, doi: 10.1088/1361-6420/ad0f3b.



**Anran Xu** received the Honours Bachelor of Science degree in Mathematics & Its Applications Specialist (Physical Science) and Physics Major from the University of Toronto, Toronto, ON Canada, in 2022. She is currently pursuing a Master of Science in Geophysics with the University of British Columbia, Vancouver, BC Canada.

Her research interests include inverse problems and machine learning applications.



**Lindsey J. Heagy** is an Assistant Professor in the Department of Earth, Ocean and Atmospheric Sciences and Director of the Geophysical Inversion Facility at UBC. She completed her BSc in geophysics at the University of Alberta in 2012 and her PhD at UBC in 2018. Prior to her current position, she was a Postdoctoral researcher in the Statistics Department at UC Berkeley.

Her research combines computational methods in numerical simulations, inversions, and machine learning to characterize the geophysical subsurface.